



Influence of the AlN interlayer thickness on the photovoltaic properties of in-rich AlInN on Si heterojunctions deposited by RF sputtering

Rodrigo Blasco, Arantzazu Núñez-Cascajero, Marco Jiménez-Rodríguez, Daniel Montero, Louis Grenet, Javier Olea, Fernando B. Naranjo, Sirona Valdueza-Felip

► To cite this version:

Rodrigo Blasco, Arantzazu Núñez-Cascajero, Marco Jiménez-Rodríguez, Daniel Montero, Louis Grenet, et al.. Influence of the AlN interlayer thickness on the photovoltaic properties of in-rich AlInN on Si heterojunctions deposited by RF sputtering. *AIP Advances*, 2018, 8 (11), pp.115315. 10.1063/1.5041924 . cea-02952499

HAL Id: cea-02952499

<https://cea.hal.science/cea-02952499>

Submitted on 29 Sep 2020

HAL is a multi-disciplinary open access archive for the deposit and dissemination of scientific research documents, whether they are published or not. The documents may come from teaching and research institutions in France or abroad, or from public or private research centers.

L'archive ouverte pluridisciplinaire **HAL**, est destinée au dépôt et à la diffusion de documents scientifiques de niveau recherche, publiés ou non, émanant des établissements d'enseignement et de recherche français ou étrangers, des laboratoires publics ou privés.



Distributed under a Creative Commons Attribution 4.0 International License

Influence of the AlInN Thickness on the Photovoltaic Characteristics of AlInN on Si Solar Cells Deposited by RF Sputtering

Rodrigo Blasco,* Arántzazu Núñez-Casajero, Marco Jiménez-Rodríguez, Daniel Montero, Louis Grenet, Javier Olea, Fernando B. Naranjo, and Sirona Valdueza-Felip

The influence of the AlInN thickness (65–145 nm) on the photovoltaic characteristics of In-rich n-Al_xIn_{1-x}N ($x \approx 0.38\text{--}0.42$) on p-Si(111) heterojunctions deposited by radio frequency sputtering has been reported. All samples show a closely packed columnar morphology with a root mean-squared surface roughness below 3.7 nm and an apparent optical bandgap energy of ≈ 2.0 eV. Dark current density–voltage curves of the solar cell devices based on the developed AlInN/Si(111) heterojunction reveal shunt and series resistances in the range of 1.3–5.0 kΩ and 7.7–16.2 Ω depending on the AlInN thickness, respectively. Their photovoltaic performance shows an enhancement with the AlInN thickness, with an increase of the short circuit current and conversion efficiency from 16 to 19 mA cm⁻² and from 1.8 to 2.5% under one-sun AM1.5G illumination. At the same time, the open circuit voltage and the fill factor remain at $\approx 0.34\text{--}0.40$ V and $\approx 30\text{--}37\%$, respectively. These effects are due to the enhanced optical transmittance of the AlInN layer in the wavelength range in which the maximum of the Si spectral photoresponse occurs, in agreement with the increased responsivity of the devices at 950 nm of 450 mA W⁻¹. These results demonstrate the feasibility of using In-rich AlInN alloys deposited by radio frequency sputtering as n-type layer of AlInN/p-type Si heterojunction solar cells.

1. Introduction

Phase separation effect are a current problem when synthesizing In-rich AlInN alloys by molecular beam epitaxy^[1–3] or metalorganic vapor phase epitaxy.^[4,5] However, the radio-frequency (RF) sputtering technique^[6–14] allows the deposition of low-cost, large-area, and single phase nanocrystalline AlInN layers, also permitting the low temperature deposition on both crystalline and amorphous substrates. It is hence an easy technology to be scaled up to industry.

It could be possible to optimize a solar cell at a desired range of the solar spectrum by just tuning the direct bandgap of AlInN which varies from InN in the near infrared (0.7 eV^[15]) to AlN in the ultraviolet (6.2 eV^[16]) only changing the alloy composition. Besides, the thermal stability and radiation hardness of III-nitrides could also improve the properties of the silicon-based heterojunctions in space applications. In this sense, the possibility of including an n-type AlInN deposited by RF sputtering on

p-type silicon for interesting topic. Liu et al.^[7] demonstrated a conversion efficiency of 1.1% in Al_{0.27}In_{0.73}N on Si(100) devices with an open circuit voltage $V_{oc} = 0.27$ V, a short circuit current density $J_{sc} = 14$ mA cm⁻², and a fill factor FF = 29%, leading to a conversion efficiency of 1.1% under one sun AM 1.5G illumination with 90 nm of AlInN using a mixture of argon and nitrogen for the deposition of the nitride layer. However, no spectral photoresponse of the device was reported in ref. [7].

In this work, we study the structural, morphological, and optical properties of Al_xIn_{1-x}N ($x = 0.38\text{--}0.42$) layers deposited under pure nitrogen atmosphere on Si(111) as a function of the AlInN thickness ranging from 65 to 145 nm. The AlInN thickness is a crucial parameter for the light collection process affecting the photovoltaic characteristics of the heterojunctions due to the high absorption coefficient of the nitride layer in the vis/UV wavelength range.

R. Blasco, Dr. A. Núñez-Casajero, M. Jiménez-Rodríguez,
Prof. F. B. Naranjo, Dr. S. Valdueza-Felip
Photonics Engineering Group
University of Alcalá
28871 Alcalá de Henares, Spain
E-mail: rodrigo.blasco@uah.es

D. Montero, Dr. J. Olea
Thin Film and Microelectronics Group
University Complutense of Madrid
28040 Madrid, Spain

L. Grenet
LITEN
CEA-Grenoble
University Grenoble Alpes
38000 Grenoble, France

 The ORCID identification number(s) for the author(s) of this article can be found under <https://doi.org/10.1002/pssa.201800494>.

DOI: 10.1002/pssa.201800494

2. Experimental Section

The $\text{Al}_x\text{In}_{1-x}\text{N}$ layers were deposited on p-doped (1.5×10^{14} – $1.5 \times 10^{16} \text{ cm}^{-3}$) 500 μm thick Si(111) substrates with a resistivity of 10–100 $\Omega \cdot \text{cm}$ using a reactive RF sputtering, equipped with 2-inch confocal magnetron cathodes of pure In (99.995%) and Al (99.999%), and pure nitrogen (99.9999%) was used as reactive gas. Substrates were chemically cleaned in organic solvents before being loaded in the deposition chamber where they were outgassed for 30 min at 550 °C. Prior deposition, targets and substrate were cleaned using a soft plasma etching with pure Ar (99.9999%) in the sputtering chamber. AlInN layers were deposited with a nitrogen flow of 14 sccm at a sputtering pressure of 0.47 Pa. The Al and In RF powers were fixed at 150 and 40 W, respectively. Samples were deposited at a substrate temperature of 550 °C. Under these growth conditions, the AlInN layer presents an n-type carrier concentration of $n \approx 2.7 \times 10^{20} \text{ cm}^{-3}$, as previously evaluated by Hall Effect measurements in samples with a thickness of 455 nm deposited under the same growth conditions on sapphire.^[14,17] A set of samples with AlInN thickness ranging from 65 to 145 nm (samples D1–D4 in Table 1) was deposited.

The alloy mole fraction, crystalline orientation, and mosaicity of the layers were obtained from high-resolution X-ray diffraction (HRXRD) measurements. To analyze the surface morphology an atomic force microscope (AFM) in tapping mode was used. A field-emission scanning electron microscope (FESEM) was employed to estimate the layer thickness and morphology. The optical properties were analyzed in AlInN layers simultaneously deposited on sapphire substrates under the same growth conditions. In these samples, the AlInN bandgap energy was estimated from transmittance measurements performed at normal incidence in the 400–1700 nm wavelength range using an optical spectrum analyzer.

Samples were processed into $\approx 1 \times 1 \text{ cm}^2$ devices to evaluate the photovoltaic performance of the heterojunction, as shown in Figure 1(a) and (b). One hundred nanometer thick Al layers were deposited by RF sputtering as top and bottom contacts to n-AlInN and p-silicon, respectively, using a shadow mask for the top contact. The former present ohmic behavior was deposited, while the latter was annealed at 450 °C during 3 min under nitrogen atmosphere to ensure an ohmic behavior. N- and p-contact resistivity of 2 ± 1 and $5.5 \pm 1.5 \Omega \cdot \text{cm}^2$ were, respectively, obtained from transmission line method measurements.

Devices were characterized by current density–voltage (J – V) curves carried out in dark and under standard illumination at

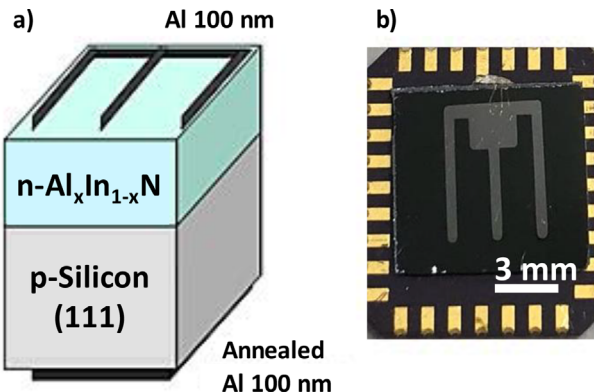


Figure 1. a) Sketch of the AlInN on Si heterojunctions. b) Top-view image of a representative processed device with a $\approx 1 \times 1 \text{ cm}^2$ area.

25 °C. Dark measurements were recorded with a four-point probe station, whereas measurements under illumination were performed in a solar simulator with a AM1.5G spectrum (100 mW cm^{-2}). The spectral response of the devices in the 400–1100 nm range was measured at zero bias using a 250 W halogen lamp coupled to a monochromator. These results were calibrated using the response of the cell to a GaN-based laser diode emitting at 405 nm with a known output power to obtain the device responsivity.

3. Results and Discussion

The structural quality of the Al_xIn_{1-x}N films as a function of their thickness was evaluated with HRXRD measurements. Figure 2 shows the diffractograms corresponding to the $2\theta/\omega$ scans of the layers. Only the diffraction peaks related to the Si (111) and the AlInN (0002) are observed independently of the AlInN thickness, pointing out non-parasitic orientations of the nitride films, with the absence of the typical multiple peaks measured in layers with phase separation. From the angle value of (0002) diffraction peak of AlInN, we estimate an Al mole fraction of $x \approx 0.38$ –0.43 assuming fully relaxed layers and applying the Vegard's law to the estimated c-parameter of the layer. We assume fully relaxed layers taking into account previous studies performed by our group and presented in ref.^[14] The applicability of the Vegard's law has been previously demonstrated by our group in similar samples grown on sapphire^[17] an error in the estimation of Al content below 3%.

Table 1. Electrical characteristics of the AlInN on Si heterojunctions versus the AlInN thickness. The area of the devices was estimated taking into account the area of the top contact ($\approx 0.13 \text{ cm}^2$).

Sample	Thickness [nm]	Area [cm^2]	Dark			One sun AM 1.5G				R at 950 nm [mA W^{-1}]
			R_{sh} [k Ω]	R_s [Ω]	J_0 [mA cm^{-2}]	V_{oc} [V]	J_{sc} [mA cm^{-2}]	FF [%]	Efficiency [%]	
D1	65	0.54	1.6	9.0	0.031	0.34	16.00	32.95	1.80	360
D2	90	0.62	1.3	8.9	0.035	0.35	15.62	33.80	1.84	–
D3	100	0.73	5.0	16.2	0.004	0.40	15.50	30.14	1.86	445
D4	145	0.52	3.3	7.7	0.012	0.34	18.79	37.76	2.45	470

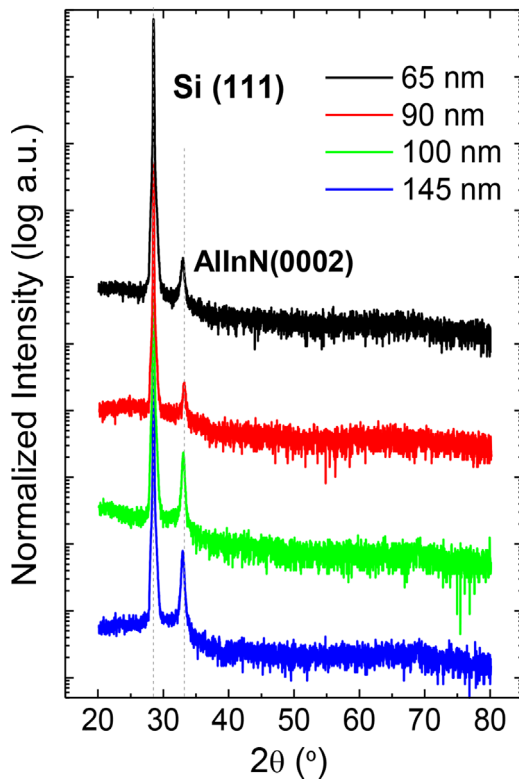


Figure 2. $2\theta/\omega$ scans of the AlInN on Si(111) structures as a function of the AlInN thickness.

The rocking curve analysis around the AlInN (0002) diffraction peak reveals a decrease of the full width at half maximum from 10° to 7° when increasing the AlInN thickness. These results are similar to those obtained for layers with 90 and 450 nm grown in similar conditions in which a value of 7° and 5° are obtained, respectively.

FESEM images depicted in **Figure 3** show a closely packed columnar morphology in all samples with a thickness of 65, 90, 100, and 145 nm for samples D1–D4, respectively. From the $2 \times 2 \mu\text{m}^2$ atomic force microscopy images of the AlInN surface, we obtain a root mean square (rms) surface roughness from 3.7 to 0.9 nm independently of the layer thickness.

Transmittance spectra of the AlInN on sapphire samples deposited under the same run are shown in **Figure 4**. It can be observed that the transmittance spectrum is influenced by the AlInN thickness, leading to a possible underestimation in the calculation of the bandgap energy. From the spectra of sample D4 with 145 nm of AlInN, we deduce an apparent optical bandgap energy of ≈ 2.0 eV, in accordance with the one obtained in 455-nm thick AlInN on sapphire grown under the same deposition conditions.^[17]

Figure 5(a) shows the J – V characteristics of the developed devices based on the analyzed heterojunctions under dark conditions showing a rectifying behavior. From these curves, we estimated the saturation current density (J_0), series and shunt resistances (R_s , R_{sh}) as summarized in Table 1. The best values are obtained for sample D4 with the lowest R_s and a relatively high R_{sh} . Even though sample D3 has a higher R_{sh} , the high

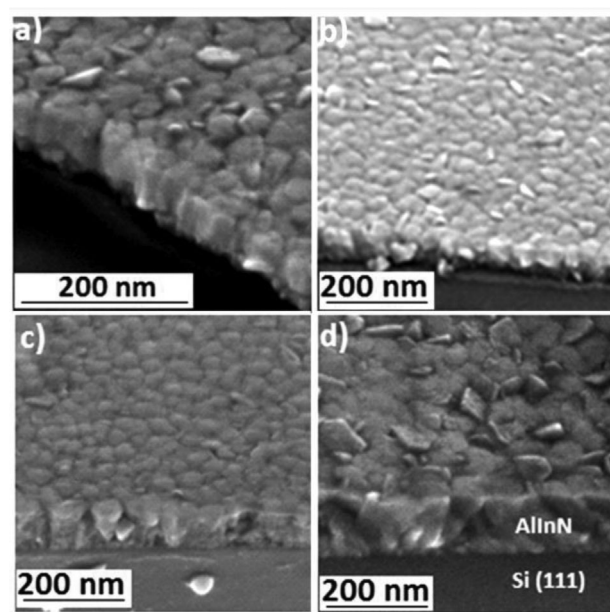


Figure 3. FESEM images of the AlInN on Si(111) structures with (a) 65 nm, (b) 90 nm, (c) 100 nm, and (d) 145 nm.

value of the dark current density J_0 is probably the responsible of the average poorer performance of this sample compared to D4. The improvement of the electrical parameters can be explained from the layer relaxation, which is happening as the layer thickness increases.^[18] The density of defects decreases with the accommodation of the layer causing a reduction of the electrical losses. The obtained values are in the same order of magnitude than the ones reported by Liu et al.^[6] of $R_s = 7 \Omega$ and $R_{sh} = 5 \text{ k}\Omega$ for AlInN on Si(100) heterojunctions deposited by RF sputtering. On the other hand, an ideality factor of $n \approx 3\text{--}8$ is obtained for all devices.

The values of V_{oc} , J_{sc} , FF and conversion efficiency estimated from J – V measurements under 1 sun AM1.5G illumination [Figure 5(b)] are summarized in Table 1. Comparing the four devices, the variations of V_{oc} from 0.34 to 0.40 V, independently

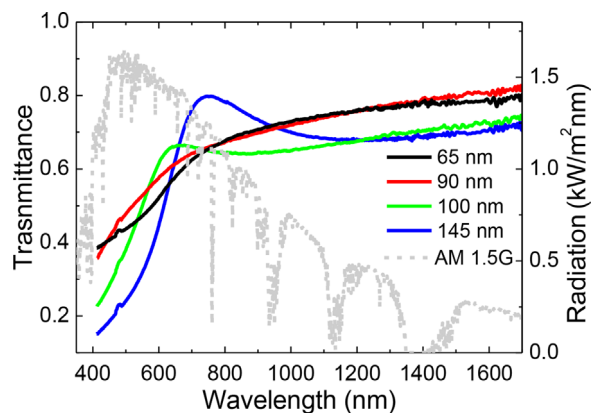


Figure 4. Normalized transmittance spectra of the AlInN on sapphire layers (left) and the solar spectrum of one sun AM 1.5G (right).

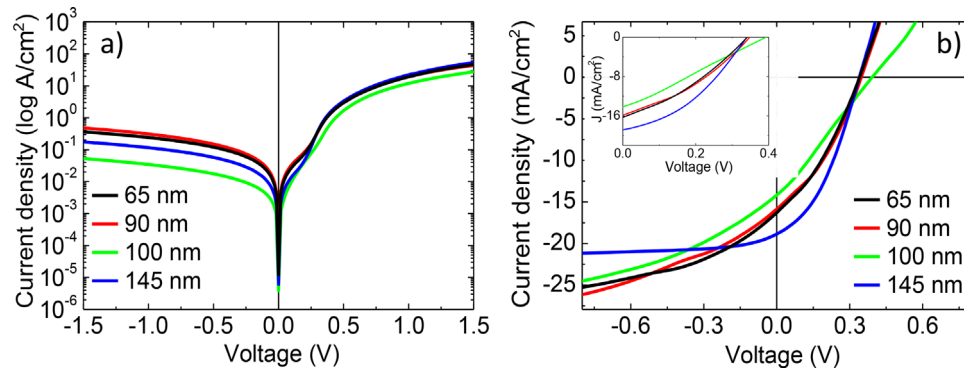


Figure 5. Current density–voltage curves of the AlInN on Si heterojunctions (a) in the dark (log scale) and (b) under 1 sun AM1.5G illumination. Inset: zoom of the fourth quadrant.

of the AlInN thickness, can be due to the variations of the Al mole fraction in the AlInN layers and the differences of R_s in the devices. On the other hand, the FF varies for all devices between 30 and 38%. However, the J_{sc} increases with the AlInN thickness from ≈ 15.5 to 18.79 mA cm^{-2} , leading to an improvement of the conversion efficiency from 1.8 to 2.45%. This positive evolution of the J_{sc} and the conversion efficiency with the AlInN thickness can be due to the improved transmittance of sample D4 in the 700–1000 nm spectral range, as observed in Figure 4, compared to their counterparts. We recall that the maximum responsivity of a standard Si-based photodetector is found in this wavelength range.

For a better understanding of these results, we have measured the responsivity of the devices, as illustrated in Figure 6. The spectral response of the samples covers the visible to near-infrared spectral range, with a peak associated to the silicon photodetection. Peak responsivity values are 360 mA W^{-1} at 930 nm, 445 mA W^{-1} at 850 nm, and 470 mA W^{-1} at 950 nm for samples D1, D3, and D4, respectively. However, if we compare the responsivity of devices D3 and D4, we observe an improved responsivity in the 500–700 nm wavelength range for D3, and in the 850–1000 nm range for D4. These results are in agreement with the increased transmittance of the AlInN layer for each

sample at the referred wavelength range (see Figure 6). This effect is attributed to the Fabry-Pérot interference pattern induced by the layer-substrate and layer-air interfaces, increasing the amount of light reaching the bottom Si layer and hence the contribution to carrier photogeneration. In the case of sample D1, the reduced transmittance of the AlInN layer leads to a reduced responsivity and conversion efficiency of the device.

4. Conclusion

The effect of the AlInN thickness (65–145 nm) on the material and photovoltaic characteristics of AlInN on Si(111) heterojunction solar cells were analyzed. The structural, morphological, and optical properties of the $\text{Al}_x\text{In}_{1-x}\text{N}$ ($x = 0.38\text{--}0.42$) layers were not strongly affected by the layer thickness, obtaining closely packed columnar films with a rms surface roughness in the range of $\approx 1\text{--}4\text{ nm}$ and an apparent optical bandgap energy $\approx 2.0\text{ eV}$. However, the photovoltaic performance of the heterojunctions improved with the thickness of the AlInN. Namely the conversion efficiency improves from 1.80 to 2.45% and the responsivity from 360 to 470 mA W^{-1} at 950 nm due to the enhanced transmittance of the AlInN layer in the wavelength range in which the maximum of the Si spectral photoresponse occurs. These results highlight the importance of the proper design of the transparency of AlInN to improve the device efficiency.

Acknowledgments

Support from projects NitPho (TEC2014-60483-R), MADRID-PV (S2013/MAE-2780), SINFOTON (S2013/MIT-2790), PhotoAI (CCG2015/EXP-014), INFRASIL (TEC2013-41730-R), TEC2017-84378-R and ANOMALOS (TEC2015-71127-C2-2-R) is acknowledged. D. Montero acknowledges the financial help coming from a FPI grant no. BES-2014-067585 provided by the Spanish Ministry of Economy, Development and Tourism partially funded by the European Social Fund.

Conflict of Interest

The authors declare no conflict of interest.

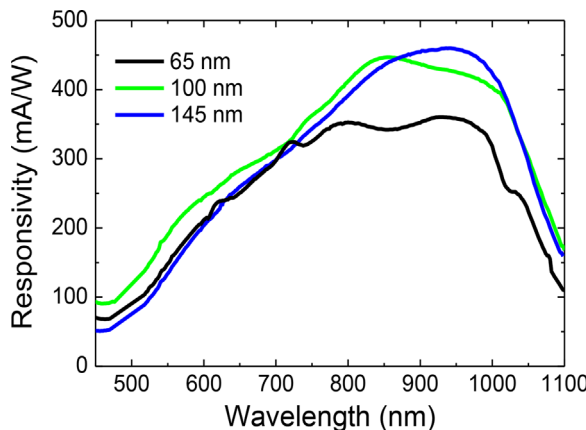


Figure 6. Responsivity of the AlInN on Si heterojunctions.

Keywords

AlInN, solar cells, sputtering

Received: June 29, 2018

Revised: July 27, 2018

Published online:

- [1] W. C. Chen, Y. H. Wu, C. Y. Peng, C. N. Hsiao, L. Chang, *Nanoscale Res. Lett.* **2014**, *9*, 1.
- [2] Y. H. Wu, Y. Y. Wong, W. C. Chen, D. S. Tsai, C. Y. Peng, J. S. Tian, L. Chang, E. Yi Chang, *Mater. Res. Express* **2014**, *1*, 15904.
- [3] J. Kamimura, T. Kouno, S. Ishizawa, A. Kikuchi, K. Kishino, *J. Cryst. Growth* **2007**, *300*, 160.
- [4] S. Yamaguchi, M. Kariya, S. Nitta, H. Kato, T. Takeuchi, C. Wetzel, H. Amano, I. Akasaki, *J. Cryst. Growth* **1998**, *195*, 309.
- [5] L. Yun, T. Wei, J. Yan, Z. Liu, J. Wang, J. Li, *J. Semicond.* **2011**, *32*, 93001.
- [6] H. F. Liu, C. C. Tan, G. K. Dalapati, D. Z. Chi, *J. Appl. Phys.* **2012**, *112*, 63114.
- [7] H. F. Liu, S. B. Dolmanan, S. Tripathy, G. K. Dalapati, C. C. Tan, D. Z. Chi, *J. Phys. D: Appl. Phys.* **2013**, *46*, 95106.
- [8] Q. Guo, T. Tanaka, M. Nishio, H. Ogawa, *Jpn. J. Appl. Phys.* **2008**, *47*, 612.
- [9] C. J. Dong, M. Xu, Q. Y. Chen, F. S. Liu, H. P. Zhou, Y. Wei, H. X. Ji, *J. Alloys Compd.* **2009**, *479*, 812.
- [10] L. F. Jiang, W. Z. Shen, Q. X. Guo, *J. Appl. Phys.* **2009**, *106*, 13515.
- [11] H. He, Y. Cao, R. Fu, W. Guo, Z. Huang, M. Wang, C. Huang, J. Huang, H. Wang, *Appl. Surf. Sci.* **2010**, *256*, 1812.
- [12] H. He, Y. Cao, R. Fu, H. Wang, J. Huang, C. Huang, M. Wang, Z. Deng, *J. Mater. Sci.-Mater. Electron.* **2010**, *21*, 676.
- [13] M. Lü, C. Dong, Y. Wang, *J. Wuhan Univ. Technol.-Mater. Sci. Ed.* **2013**, *28*, 868.
- [14] A. Núñez-Casajero, L. Monteagudo-Lerma, S. Valdueza-Felip, C. Navío, E. Monroy, M. González-Herráez, F. B. Naranjo, *Jpn. J. Appl. Phys.* **2016**, *55*, 05FB07.
- [15] J. Wu, W. Walukiewicz, K. M. Yu, J. W. Ager, E. E. Haller, H. Lu, W. J. Schaff, Y. Saito, Y. Nanishi, *Appl. Phys. Lett.* **2002**, *80*, 3967.
- [16] W. M. Yim, E. J. Stofko, P. J. Zanzucchi, J. I. Pankove, M. Ettenberg, S. L. Gilbert, *J. Appl. Phys.* **1973**, *44*, 292.
- [17] A. Núñez-Casajero, S. Valdueza-Felip, L. Monteagudo-Lerma, E. Monroy, E. Taylor-Shaw, R. W. Martin, M. Gonzalez-Herraez, F. B. Naranjo, *J. Phys. D: Appl. Phys.* **2017**, *50*, 065101.
- [18] A. G. Bhuiyan, A. Hashimoto, A. Yamamoto, *J. Appl. Phys.* **2003**, *94*, 5.